nature communications

Article

https://doi.org/10.1038/s41467-025-60316-0

Elucidating the molecular structural origin of efficient emission across solid and solution phases of single benzene fluorophores

Received: 30 August 2024

Accepted: 20 May 2025

Published online: 01 July 2025

Check for updates

Jung-Moo Heo[1], Jihyun Park[2], Maria F. Flórez-Angarita[3,4], Liangxuan Wang[3,5], Changhoon Yu[1,6], Jinho Choi[1], Hochul Woo[2,7], Begoña Milián-Medina[4], Adam J. Matzger[2,7], Min Sang Kwon[6] ✉, Johannes Gierschner[3] ✉ & Jinsang Kim[1,2,7,8] ✉

Achieving high quantum yields for organic fluorophores in both solution and in the polycrystalline solid state is a significant yet challenging goal, as most fluorophores typically emit effectively in only one phase. In this study, we introduce 1,1′-(2,5-dimethoxyterephthaloyl)-bis(glutraimide) (TGlu), a novel 'single benzene'-based organic fluorophore featuring an alkoxy donor and an *N*-acyl-glutarimide acceptor. TGlu achieves close-to-unity fluorescence quantum yields in both solution and in the polycrystalline state. Through systematic studies involving four additional structural analogues of TGlu, we unveiled that the acceptor group within the single benzene core plays a crucial steric and electronic role in achieving high fluorescence efficiency in both phases. Furthermore, we demonstrated the versatility of this new fluorophore in various applications. In solution, TGlu serves as a highly effective photocatalyst for photoinduced energy/electron transfer reversible addition–fragmentation chain-transfer polymerization while in its single-crystal form, TGlu exhibits highly efficient waveguiding properties.

Organic fluorescent materials have garnered significant attention due to their pivotal role in various crucial applications, including fluorescent probes for bioimaging[1,2], photocatalysis[3,4], organic light-emitting devices[5], laser technology[6,7], and others[8–11]. To ensure that materials perform effectively across various applications, it is essential to tune and optimise their properties, such as the extinction coefficient, colour, bandwidth, fluorescence lifetime (τ_F), and particular the quantum yield (Φ_F)[7,12–14].

The selection of highly fluorescent organic materials is primarily guided by their intended application. Notably, the choice of fluorophore core structure is heavily influenced by whether the application occurs in the solution phase or in the solid state, as the fluorescence of many compounds are quenched either in fluid solution or in the solid state[12,15,16]. For instance, extended π conjugated dyes (e.g., polyaromatic hydrocarbons, coumarins and xanthene dyes, etc) are highly emissive in solution; however, they experience significant fluorescence quenching in the poly- or nano-crystalline solid state, mainly due to trap-controlled emission quenching[12,17] (or, in some cases, by singlet fission[18]), see Supplementary Fig. 1 and Supplementary Table 1. Nevertheless, single crystals of these dyes typically display high Φ_F, proving that the

[1]Department of Materials Science and Engineering, University of Michigan, Ann Arbor, Michigan, USA. [2]Department of Chemistry, University of Michigan, Ann Arbor, Michigan, USA. [3]Madrid Institute for Advanced Studies, IMDEA Nanoscience, Calle Faraday 9, Campus Cantoblanco, Madrid, Spain. [4]Department for Physical Chemistry, Faculty of Chemistry, University of Valencia, 46100 Burjassot, Valencia, Spain. [5]Institute of Physical and Theoretical Chemistry, Eberhard Karls University Tübingen, Auf der Morgenstelle 18, Tübingen, Germany. [6]Department of Materials Science and Engineering, Research Institute of Advanced Materials, Seoul National University, Seoul, Republic of Korea. [7]Macromolecular Science and Engineering, University of Michigan, Ann Arbor, Michigan, USA. [8]Biointerfaces Institute, University of Michigan, Ann Arbor, Michigan, USA. ✉e-mail: minsang@snu.ac.kr; johannes.gierschner@imdea.org; jinsang@umich.edu

quenching observed in the polycrystalline phases is usually not "aggregation caused", but "trap-controlled"[12]. Conversely, some compound families like α-cyanostilbenes[12,19–21] or tetraphenylethenes[12,22,23] display weak emission in solution but exhibit enhanced emission in the solid state. In most cases, this is due to the restricted environment (i.e., also observed in solid or frozen solution), which blocks the access to the conical intersection (CI) and thus suppresses the nonradiative decay[12,23–25]. Therefore, this is "aggregation-induced" (as expressed in the AIE terminology) in only a trivial sense, and can be better termed, in a physically sound way, as solid-state luminescence enhancement (Supplementary Fig. 2)[12,20]. Despite ongoing efforts, fluorophores with high Φ_F in both solution and in polycrystalline solid phases remain still rare[12,15,16,19]. It is noted that these "solution and solid-state emitters" (SSSEs)[16] are sometimes called "dual state emitters", which is, however, easily confused with the well-established "dual emitters"[26]. While there is no universally defined threshold for SSSEs, we adopt the practical classification of $\Phi_F \geq 5\%$ in both solution and solid states[27]. SSSE fluorophores can significantly simplify the design and selection process, reduce trial and error, and ultimately save time and effort in fluorophore development.

One effective strategy for achieving SSSE systems utilises donor-acceptor (DA) substituted single benzene rings as the core structure, now often called "single benzene fluorophores" (SBFs)[28–53]. Early examples for SBFs include the intensively studied p-dimethylaminobenzonitrile (DMABN) and its derivatives, which are known for their ability to emit visible light[54]. Different to DMABN and related compounds with such dipolar *para*-DA motif, however, modern SBF fluorophores typically use an alternating *ortho*,*meta*- (*o*,*m*-)bis-DA motif, early introduced by Baeyer[30,55,56]; this gives rise to inversion symmetry and thus to a quadrupolar structure (Fig. 1a). We remind in this context that DA-based quadrupolar fluorophores can provoke substantial intramolecular charge transfer (ICT) of the emitting state[57,58], as ICT is not an exclusive property of dipolar DA systems[12,59]. The ICT character of quadrupolar compounds generally gives rise to (i) bathochromic shifts of varying amounts[57,58], (ii) enhanced Stokes shifts (ΔE_{Stokes}) between absorption and emission[57], and (iii) decreased oscillator strengths (and, thus, extinction coefficients) of the emitting state[57,58], while occasionally maintaining a high Φ_F[58,59]. These features are also observed for the mentioned quadrupolar *o*,*m*-bis-DA-type SBF dyes, generating tunable visible light emission, and usually large ΔE_{Stokes}[30]. Among the different suggestions to explain the large ΔE_{Stokes}, even antiaromaticity was recently hypothesised[34,35]. We note in this context that the large ΔE_{Stokes} of benzene itself is not related to antiaromaticity. In contrast to polycyclic aromatic hydrocarbons, the S_1 state of benzene is symmetry-forbidden, so that the emission is governed by Herzberg-Teller (HT) coupling, which gives rise to the large ΔE_{Stokes}. In general, the understanding of ΔE_{Stokes} in molecules with ICT character requires a full vibronic treatment including HT and (linear and quadratic) FC contributions, as well as inclusion of implicit solvent effects. Nonetheless, antiaromaticity does not explain the strong bathochromic shifts of *o*,*m*-bis-DA-type SBFs against other positional isomers, which are not only present in emission but already in absorption. Such positional DA isomer considerations were early established for DA-substituted benzenes[60,61], and will be crucial in the current context (*vide infra*); in fact, by now, they were not consequently pursued in the current SBF literature.

Notably, non-radiative decay pathways in solution remain present in SBFs, depending on the substituent structure, so that Φ_F typically ranges from about 5% to 80% in solution (Supplementary Table 2). Furthermore, fluorescence quenching in polycrystalline solids is an imperative challenge, which can be overcome by rationally designed bulky substituents (Supplementary Fig. 3)[36–38]. High solid state Φ_F for these materials can be traced back to the reduction of exciton coupling by quasi-isolated intermolecular arrangements[12]; the latter prevents effective exciton diffusion to the trap sites[12,17]. This approach generated SBF-SSSE fluorophores with Φ_F of about 30% or more in both solution and solid phases so far[36–38]. However, Φ_F exceeding 90% in both phases are still lacking (Supplementary Table 2).

In this study, we report a novel SBF-based SSSE-active organic fluorophore, TGlu, featuring an alkoxy donor and an *N*-acyl-glutarimide (Ac-Glu) acceptor, which achieves quantum yields exceeding 90% in both solution and solid phases (Fig. 1a). To uncover the molecular basis for these high quantum yields, we synthesised four analogues (TSuc, TPid, TPip, SGlu) with the same donor but somewhat

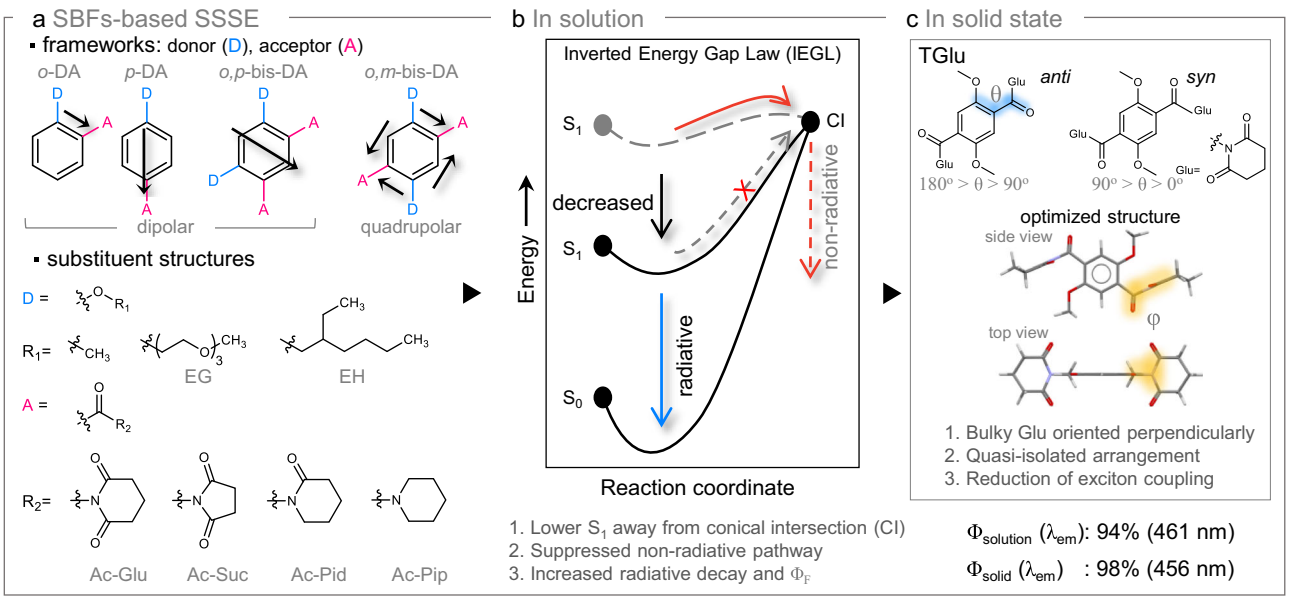

Fig. 1 | High-efficiency solid–solution emission in SBFs-based fluorophores. **a** SBFs-based SSSE-active organic fluorophores, demonstrating highly emissive properties in both solution and solid phases as developed in this work. **b** In solution, schematic surface energy diagram for excited state deactivation through an invariant CI, giving rise to the Inverted Energy Gap Law (IEGL). **c** In solid state, DFT optimisation indicates that the bulky Glu (side group) oriented perpendicularly prevents trapping and conserves the high fluorescence quantum yield (Φ_F).

https://doi.org/10.1038/s41467-025-60316-0

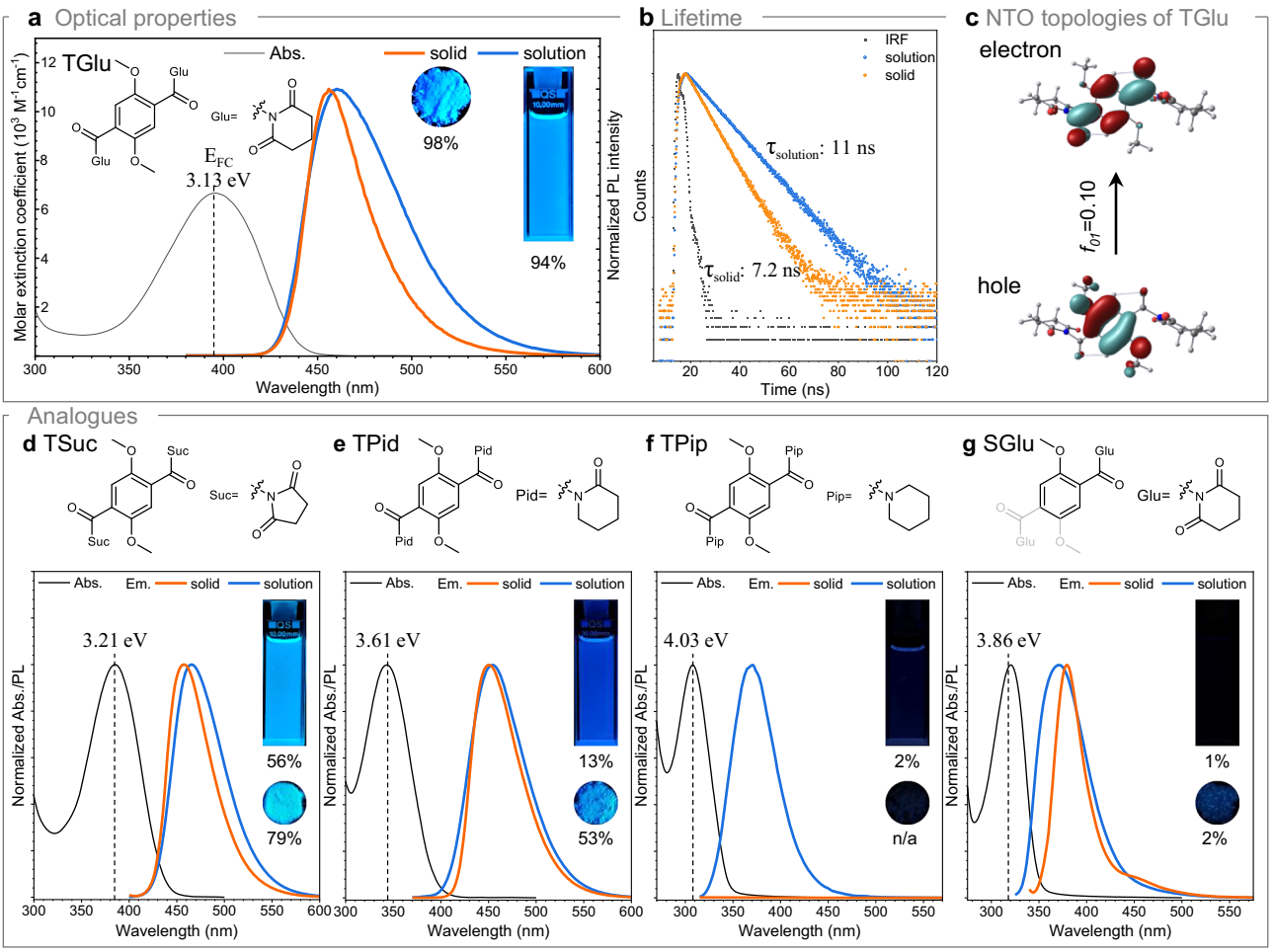

Fig. 2 | Optical properties of the investigated derivatives. a Absorption (black line), emission spectra and **b** fluorescence lifetime decay of TGlu in both solution (blue) and solid state (orange). **c** The natural transition orbital (NTO) topologies of TGlu exhibit the partial charge transfer (CT) nature. The analogues absorption and emission spectra of TSuc (**d**), TPid (**e**), TPip (**f**), and SGlu (**g**). The inset photo images under 365 nm irradiation in solution and solid state.

different acceptors (Fig. 1a). Interestingly, in solution, these fluorophores exhibit an inverted energy gap law (IEGL) behaviour; that is, the smaller the optical gap between ground and excited state, the higher becomes Φ_F[20,62]. IEGL behaviour is expected, if the variation of the Franck-Condon energy is stronger than that of the conical intersection (CI), which drives the nonradiative decay via internal conversion, see Fig. 1b[20,48]. The IEGL is particularly observed in compound families with a common core motif, in which the geometrical reorganisation towards the CI takes place. We note that the geometry change, along which the path to the CI proceeds, varies largely among different families of compounds[20,62–66]. The multireference character of the CI requires a computational treatment beyond standard density functional theory (DFT); for instance, by CASSCF/CASPT2[20,63,64], or (more cost-effective) by mixed-reference spin-flip time-dependent DFT (MRSF-TD-DFT)[65], or by excited state non-adiabatic molecular dynamics[66].

The CI model is suggested to hold for the molecules in the present study as well, being responsible for the high Φ_F of 94% for TGlu in fluid solution. Moreover, the bulkiness of the acceptor moiety in TGlu prevents trapping[12,17], and thus conserves the very high Φ_F also in the polycrystalline solid phase, with a remarkable 95% and narrow bandwidth (Fig. 1c). Thanks to its high quantum yields in both phases, TGlu exhibits high efficiency as a photocatalyst for photoinduced energy/electron transfer reversible addition–fragmentation chain-transfer (PET-RAFT) polymerisation and also demonstrates excellent waveguiding efficiency.

Results

Design, synthesis and solid state preparation

We have designed a blue emitting fluorophore (1,1′-(2,5-dimethoxyterephthaloyl)bis-(glutarimide) (TGlu) as shown in the inset of Fig. 2a. Considering previously reported SBFs, we structured TGlu with two methoxy donor (D) and two *N*-acyl-glutarimide (Ac-Glu) acceptor units (A), so that each D-A (D-D, A-A) moieties are in ortho (para) position (cf. Fig. 1a), which results in an overall quadrupolar moment; the latter is indeed confirmed by the DFT calculations, which gave no permanent dipole moment. TGlu can be synthesised on a gram scale without complicated protocols, enhancing their practical applicability (see the details in Supplementary Fig. 34). The bulky Ac-Glu acceptor is designed to restrict molecular motions and to prevent strong exciton coupling caused by molecular aggregation, thereby minimising nonradiative quenching pathways in the solid state (*vide infra*). To gain further evidence for our hypothesis, we optimised TGlu at the DFT level of theory; we note that here two rotamers for the torsion θ around the C_{aryl}-$C_{carbonyl}$ bond are possible, that is with in *anti* (180° > θ > 90°) or *syn* (90° > θ > 0°). According to the DFT calculations of the free molecule in vacuum, the *anti*-rotamer is slightly more stable with a planar conformation (θ = 180°; see Fig. 1); the *anti*-rotamer is also found experimentally in the solid state (*vide infra*). At the same time, the Glu moieties are oriented perpendicular to the plane, see Fig. 1c. This conformational locking, both in the ground and first excited state (S_0, S_1), is further seen in the rigid scan for the rotation of the Glu group (torsional angle φ), displaying narrow, steep potential

Table 1 | Photophysical Properties of the Investigated Derivatives in the different phases

Compounds	Phase	λ_{abs} (nm)	E_{FC} (eV)	ε (10^3 M^{-1} cm^{-1})	λ_{em} (nm)	ΔE_{stokes} (eV)	Φ_F (%)[a]	τ_F (ns)[b]	k_F (10^7 s^{-1})	k_{nr} (10^7 s^{-1})
TGlu	solution	395	3.13	6.7	461	0.45	94	11[c]	8.5	0.5
	polycrystalline	–	–	–	456	–	98	7.2[c]	14	0.3
	single crystal	–	–	–	462	–	54	6.3[c]	8.6	7.3
TSuc	solution	386	3.21	5.5	469	0.57	56	12[c]	4.6	3.6
	polycrystalline	–	–	–	457	–	79	4.7[c]	17	4.5
TPid	solution	343	3.61	3.8	450	0.87	13	3.3[c]	3.9	26
	polycrystalline	–	–	–	454	–	53	7.0[c]	7.6	6.7
TPip	solution	308	4.03	4.2	383	0.79	2	2.8[d]	0.71	35
	polycrystalline	–	–	–	–	–	–	–	–	–
SGlu	solution	321	3.86	5.4	371	0.52	1	1.4[d]	0.71	71
	polycrystalline	–	–	–	377	–	2	–	–	–

Absorption maximum λ_{abs} and E_{FC}, molar extinction coefficient ε, emission maximum λ_{em}, fluorescence quantum yield (Φ_F) and lifetime (τ_F), radiative ($k_F = \Phi_F/\tau_F$) and nonradiative rates ($k_{nr} = (1-\Phi_F)/\tau_F$). The absorption and emission wavelengths are noted at their maximum peaks. [a] Absolute quantum yields were measured using an integrating sphere. The absorption and emission data within the integrating sphere were compared with those of a blank sample. Each sample was tested in quadruplicate, using a freshly prepared sample for each quantum yield measurement to ensure consistency. All measurements demonstrated high repeatability, and the reported errors are given as ±1 standard deviation. [b] Lifetimes (τ_F) were measured by time-correlated single-photon counting (TCSPC) in Supplementary Fig. 15. The τ_F are extracted from [c] mono-exponential fits: $I(t) = A\times\exp(-t/\tau_F)$ and [d] bi-exponential fits: $I(t) = A_1\times\exp(-t/\tau_1) + A_2\times\exp(-t/\tau_2)$ and $\langle\tau_F\rangle_{int} = (A_1\times\tau_1^2 + A_2\times\tau_2^2)/(A_1\times\tau_1 + A_2\times\tau_2)$.

energy surfaces (PESs) for rotation around φ, see Supplementary Fig. 4. As we will discuss further down, these structural factors play a decisive role for the emissive character of the compound.

To gain further insight into the molecular origin of high fluorescence efficiency of TGlu (*vide infra*), we prepared four structural analogues with the same donor and slightly different acceptors: TSuc, TPid, TPip and SGlu, varying electronic and steric properties (as shown in the inset to Fig. 2d–g). We then investigated the optical properties (absorption and emission spectra) and photophysical properties (Φ_F, τ_F) of the compounds both in solution (chloroform) and in the solid phase; the latter was prepared as polycrystalline powders by a fast evaporation method from dichloromethane; for TGlu, also a single crystal was grown by slow solvent evaporation from a mixture of ethyl acetate and ethanol (see Supplementary Fig. 5).

Photophysical properties in solution

In chloroform solution, TGlu exhibits an absorption maximum at 395 nm, an intense sky blue fluorescence at 461 nm (corresponding to $\Delta E_{Stokes} = 0.45$ eV), with a high quantum yield (Φ_F) of 94%, a full width at half maximum (FWHM) of 0.33 eV (58 nm), and a long lifetime (τ_F) of 11 ns (see Fig. 2a for the UV/Vis absorption and emission spectrum, and Fig. 2b for the decay). The long τ_F is caused, on one hand, by a small radiative rate of 8.5×10^7 s^{-1} (obtained via $k_F = \Phi_F/\tau_F$, see Table 1), which indicates a moderately small oscillator strength *f* of the emitting state[12]. This agrees with our time-dependent DFT (TD-DFT) results, which gives $f_{01} = 0.10$ for the $S_0\rightarrow S_1$ transition of TGlu, see Fig. 2c. On the other hand, the nonradiative rate, $k_{nr} = (1-\Phi_F)/\tau_F$, is very small ($0.5\times10^7$ s^{-1}), indicating that non-radiative decay pathways, as internal conversion (IC) (via a CI) or intersystem crossing (ISC) to the triplet manifold, are effectively suppressed, resulting in the high Φ_F despite the long singlet decay time of 11 ns. We note that rigidification of the environment by freezing the solution (Supplementary Fig. 6) or embedding in poly(methyl methacrylate) (sold solution; Supplementary Fig. 7) does not further increase Φ_F.

The emission properties are not strongly affected by the solvent polarity and viscosity across largely varying solvents (Supplementary Figs. 8 - 11). The emission (absorption) maxima range from 450 nm (386 nm) in cyclohexane to 488 nm (399 nm) in ethylene glycol (Supplementary Table 3). Despite these variations, TGlu solutions exhibited high Φ_F, (and consistent Φ_F); a notable exception is DMSO ($\Phi_F = 2\%$), which points to specific solute-solvent interactions that are currently under investigation in our labs. Furthermore, the hypsochromically shifted emission and absorption for cyclohexane shows a significant reduction in Φ_F with 71%; we'll return to this point further down.

The moderate emission shift vs. absorption is consistent with the quadrupolar nature of TGlu, where large solvent shifts are not expected in comparison with dipolar DA-systems[67]. In fact, the emitting state exhibits partial ICT character, as seen in the natural transition orbital (NTO) topologies given in Fig. 2c. The partial ICT character is also one factor for the moderately large Stokes shift of $\Delta E_{Stokes} = 0.45$ eV (3600 cm^{-1}) between absorption and emission[57], besides broadening through out-of-plane vibronic coupling (*vide infra*)[68,69].

The visible light emission of TGlu can be understood on the basis of simple frontier molecular orbital (FMO) considerations, since the $S_0\leftrightarrow S_1$ electronic transition of TGlu corresponds to a simple (de)excitation between the highest occupied and lowest unoccupied MOs (HOMO, LUMO; see Supplementary Table 5). For this, we compare TGlu (which corresponds to an *o*,*m*-bis-DA substituted benzene; i.e., a quadrupolar compound with C_{2h} symmetry) with the *o*,*p*-bis-DA compound (dipolar, C_{2v}). As seen in Fig. 3a, o,m-bis-DA substitution leads to a significantly smaller HOMO-LUMO gap (ΔE_{HL}) in comparison with the *o*,*p*-bis-DA compound; this complies with the expectations of the empirical "Caliezi rule," early established for these systems[60,61]. One reason for this smaller ΔE_{HL} is surely the significantly larger ICT character for the *o*,*m*-bis-DA compound in comparison with *o*,*p*-bis-DA (as easily visible in the FMOs in Fig. 3a), despite the quadrupolar character of the former. We note that such positional isomer effects were early established for DA-benzenes[60], predicting ΔE_{HL} as *m*-DA ≈ *o*-DA <*p*-DA, in agreement with experiment, but in contrast to resonance considerations[60,61]. Nevertheless, the ICT character was shown to be insufficient to explain excited-state stabilisation for multiple-DA substitution[70]. Consequently, we ascribe the additional bathochromic effect of *o*,*m*-bis-DA to a di(allyl radical) resonance contribution; the latter indeed corresponds to the LUMO topology, and cannot be drawn for the *o*,*p*-bis-DA isomer, see Fig. 3a. The theoretical considerations for *o*,*m*-bis-DA vs. *o*,*p*-bis-DA are consistent with our experimental results on the *o*,*p*-isomer of TGlu (*iso*-TGlu), see Supplementary Fig. 14; the absorption (emission) maximum of the latter is found at 321 nm (350 nm), i.e., showing a hypsochromic shift of about 0.7 eV (0.9 eV) against TGlu. At the same time, *iso*-TGlu exhibits a much lower Φ_F with only 1% in solution (8% in the solid state); we will return to this point further down. These results highlight the superior performance of the quadrupolar DA architecture in TGlu, which reduces

https://doi.org/10.1038/s41467-025-60316-0

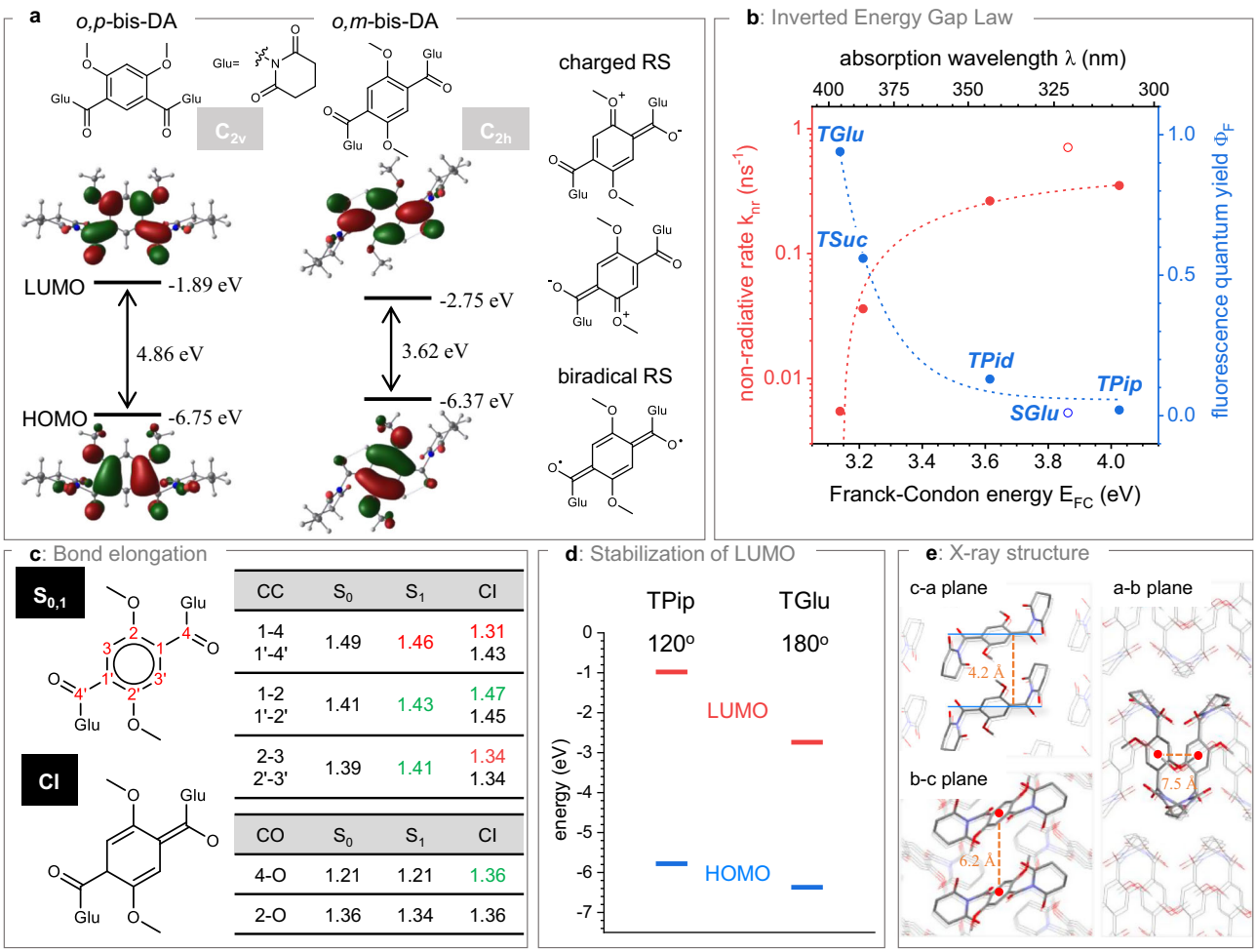

Fig. 3 | Structural and energetic factors controlling emission in derivatives. **a** Time-dependent density functional theory (TD-DFT) calculations for multiple donor-acceptor (DA) structures with differently positioned TGlu, including their resonance structures. **b** Correlation of the non-radiative rate constants (k_{nr}) and fluorescence quantum yield (Φ_F) vs their Frank-Condon energy (E_{FC}). **c** Bond elongation of the common structural unit in the excited state compared to the ground state. **d** Frontier molecular orbital (MO) energies of TGlu and TPip. **e** Structural analysis through single-crystal X-ray diffraction, showing separation distance.

the energy gap, enhances ICT, and minimises non-radiative decay pathways.

In order to understand the suppression of the nonradiative decay channel in TGlu, we further investigated four compounds, which share the D-A core motif but vary the molecular structure in a systematic manner. Starting from TGlu, we first replaced the Glu moiety by Suc (giving TSuc), then we removed one (two) carbonyl functionalities in Glu, giving TPid (TPip), finally we removed one D and A moiety, giving SGlu (as shown in the insets to Fig. 2d–g). These variations allow to systematically investigate how the number and (electronic and steric) nature of D and A impact the overall optical and photophysical properties of the molecules.

As shown in the Fig. 2d–g, we observed a bathochromic shift in absorption and emission when going from SGlu ($\lambda_{abs.}$ = 321 nm; $\lambda_{em.}$ = 371 nm) and TPip (308 nm; 383 nm) via TPid 343 nm; 450 nm) and TSuc (386 nm; 469 nm) towards the target compound TGlu (395 nm; 461 nm). At the same time, the quantum yields in solution increase systematically as 1, 2, 13, 56 and 94% in the same order (i.e., SGlu, TPip, TPid, TSuc and TGlu), respectively. Plotting k_{nr} and Φ_F against the Franck-Condon energy (E_{FC}, which corresponds, in a first approximation, to λ_{abs}[71]), we observed an unusual trend in the correlation between E_{FC} and k_{nr} (or Φ_F) in solution as shown in Fig. 3b. In fact, the smaller E_{FC} the larger Φ_F and the smaller k_{nr}; we further note that also *iso*-TGlu (E_{FC} = 3.86 eV, Φ_F = 0.01) agrees very well with this trend. This behaviour goes against the common energy gap law (EGL), and thus indicates that k_{nr} cannot be derived on the basis of Fermi's Golden Rule[72]. Instead, such inverted EGL (IEGL) was earlier ascribed to the appearance of a conical intersection (CI) at the S_0/S_1 PES[20,62,65]; here, for a given series of structurally related compounds, E_{FC} largely varies, but the CI energy is essentially invariant, see Fig. 1b[20,62,63,65]. The CI invariance was ascribed to the localised electronic nature in that region of the molecule, where the structural change on the path towards the CI proceeds; the latter was in fact found to be the structural moiety which is inherent to all compounds of the given series[62–66].

Such an inherent common structural unit is indeed present in the SBF series, depicted in Fig. 3c. In S_0, the benzene core is found to be delocalised, while the carbonyl groups are connected via single bonds, d_{14} = 1.49 Å, according to the DFT calculations. In the S_1 state the d_{12} ($d_{1'2'}$) bonds are somewhat elongated due to the presence of the DA motif[35], while d_{14} ($d_{1'4'}$) shortens. These changes are consistent with the change of the bonding character in the HOMO and LUMO, see Fig. 3a (such considerations were recently detailed for different compound families[73,74]). This is associated to the dominance of polar and biradical resonant structures in S_1 (*vide supra*), while neutral resonant structures dominate S_0, see Fig. 3c. These changes upon $S_0 \rightarrow S_1$ excitation open the path towards the CI. In fact, according to our MRSF-TD-DFT

calculations (see **Supplementary Information** for details), the CI geometry of TGlu exhibits a quinoid structure, where d_{14} shortens to 1.31 Å, while $d_{1'4'}$ stays long with 1.43 Å (Fig. 3c), reflecting broken symmetry in the CI. As this structural feature of the core is inherent to all compounds reported here, the energetics of the CI are expected to vary less with respect to those in the FC energies. In order to investigate this, we compared TGlu (i.e., highly emissive), with the symmetrical low-emissive compound, TPip (see **Supplementary Information** for details). In particular, we observe that for TGlu the CI is clearly above the FC point by $\Delta E \approx 0.3$ eV, while for TPip the CI is clearly below ($\Delta E \approx -0.5$ eV) (Supplementary Fig. 16). Therefore, access to the CI is expected to be inhibited for TGlu, while the CI is expected to be easily accessible for TPip. The theoretical results thus fully rationalise, in a qualitative manner, the experimental observation on the IEGL behaviour.

As the $S_0 \rightarrow S_1$ electronic transition corresponds to the HOMO→LUMO excitation in all cases, again, simple and illustrative FMO considerations are sufficient to understand the energetic stabilisation within the series of SBF compounds due to the one-electron description of the lowest excited state (see Supplementary Table 4). Figure 3d compares the frontier MO energies of TGlu with that of TPip, showing a much stronger stabilisation of the LUMO of TGlu than the HOMO. In the first place, this stabilisation has a geometrical component, as the core of TGlu is completely planar ($\theta = 180°$; in *anti*-conformation), while that of TPip is twisted (120°). To investigate this effect, we did a rigid scan for TGlu around θ (i.e., on both sides of the molecules, thus keeping the C_2 symmetry; see Supplementary Fig. 18), which indeed shows a significant effect of the torsional angle on the HOMO, LUMO, and bandgap. Nevertheless, this explains only partly the large stabilisation of the LUMO in TGlu. We thus evoke an additional electronic effect, enhanced resonance stabilisation (ERS)[68], considering the presence of a larger number of zwitterionic resonance structures in TGlu compared to TPip (Supplementary Fig. 19). In all, the TD-DFT calculations reproduce well the observed trends of the experimental FC energies, allowing for a rationalisation of geometrical and electronic contributions, which constitute the IEGL in the series of SBF compounds. Notably, further evidence for the IEGL arises from the experimental solvent dependence of TGlu fluorescence; while in more polar solvents Φ_F is high, as discussed (> 85%), solvation in nonpolar cyclohexane reduces Φ_F to 71% (see Supplementary Fig. 11). This is accompanied by a bathochromic shift of absorption to 386 nm (Supplementary Fig. 8); according to Fig. 3b we thus expect a notable decrease in Φ_F in good agreement with experiment. We note in this context that solvent-dependent IEGL behaviour was previously reported for merocyanines[64]; the appearance of such behaviour across different compound families thus points to a rather general concept.

Besides the mechanistic understanding of excited state deactivation, the series of SBF allows for a systematic insight into the origin of the Stokes shift ΔE_{Stokes}; the latter decreases largely from TPid (0.87 eV) via TPip, TSuc, SGlu to TGlu (0.45 eV), see Table 1. Actually, ΔE_{Stokes} is directly related to the spectral bandshapes[12], which in turn are determined by solvent broadening and effective vibronic coupling (VC)[68,69,75,76]. For symmetry-allowed electronic transitions (as in the current case), VC contains linear coupling (LC) by symmetry-allowed in-plane modes, and quadratic coupling (QC) by out-of-plane modes[68,69,75]. LC is mainly influenced by the geometry change upon electronic (de-)excitation, especially in the bond length Δ_{BL} (as recently demonstrated for colour-pure emitters[73,74]), and is therefore also sensitive to the amount of ICT character of the electronic transition. In order to investigate the influence of the substituents, we performed unbiased full vibronic TD-DFT calculation on the inherent conjugated core structure (TMe; i.e., substituting Glu in TGlu by CH_3); TMe shows substantial vibronic coupling, resulting in $\Delta E_{Stokes} = 0.44$, and with visible vibronics even at room temperature; see Supplementary Fig. 20. This indicates that the unstructured features of the experimental spectra are arising due to the presence of QC coupling of the substituents; notably, for TGlu, this does not increase ΔE_{Stokes} as the latter is the same for TGlu and TMe. Such behaviour is observed in cases, when the distortion of the QC modes upon electronic (de) excitation is small[68,69]; in fact, the frequency for the torsional mode of the Glu group is almost identical in S_0 (23 cm^{-1}) and S_1 (26 cm^{-1}), arising from the very similar PES profiles for the rotation φ in S_0 and S_1 (*vide supra*) see Supplementary Fig. 4. As a counter example we calculated TPip with a large ΔE_{Stokes} of 0.79 eV; here the distortion is indeed considerable between S_0 (64 cm^{-1}) and S_1 (103 cm^{-1}); this implies an asymmetric broadening of the spectra, and thus an increase of ΔE_{Stokes}[68,69].

Photophysical properties in solids

The emission spectrum in the polycrystalline TGlu shown in Fig. 2a is very similar to that in solution, indicating an overall small impact of intermolecular interactions in the solid[12]. This is, in fact, expected by our molecular design concept, introducing bulky acceptors to generate quasi-isolate solid state emitters[12,21]. It is particularly noticed that the onset emission is identical to solution, indicating an effective shielding of the core units from contacting each other, so the local polarizability is the same in solution and the solid state[12,31]. All this can be directly be seen in the x-ray structure of TGlu shown in Fig. 3e, which shows one-dimensional slipped stacks of well-separated molecules (in the *anti*-conformation; $\theta = 156°$) with an inter-plane separation of 4.2 Å (corresponding to displacements of 6.2 Å along the b-c plane and 7.5 Å along the a-b plane). This diminishes specifically the exciton coupling between the chromophores, a crucial factor for the exciton diffusion length, which in turn is responsible for reaching trap sites for fluorescence quenching[12,17]. Therefore, the quasi-isolate nature of TGlu in the solid state is expected to suppress fluorescence quenching; this is indeed the case, as TGlu maintains its high Φ_F in solution also in the solid state, reaching unity (98%; see Table 1) in the polycrystalline state. We note a significant drop in Φ_F for the measured single crystal vs. the polycrystalline sample, which goes against the general trend in organic materials[12,17]; this, however, must be described to the strong reabsorption in the large single crystal (ca. 1 cm) used in the measurement. Intramolecular factors, on the other hand, are expected to play a minor role for TGlu, as our experiments in solid solution had demonstrated. Conversely, TSuc and TPid exhibit markedly enhanced Φ_F in the solid state (Fig. 2d, e). For the sterically less demanding compounds TPip, SGlu with, at the same time, high E_{FC}, the path proceeds essentially barrierless towards the CI, so that these compounds show very low emission also in the solid state.

In all, the solution and solid state photophysical studies verify our suggested design concept. The intense blue emission of TGlu with close-to-unity Φ_F both in solution and the solid state, as well as CIE coordinates of (0.138, 0.08) and the narrow FWHM of 0.22 eV (38 nm) in the solid (Fig. 2a), makes TGlu an interesting compound for a wide range of practical applications.

Design of EH-TGlu and EG-TGlu

To enhance the solubility and potential applications of the core TGlu structure in various environments, we designed EH-TGlu and EG-TGlu. These compounds incorporate different alkoxy donors along with bulky hydrophobic and hydrophilic moieties (as shown in the inset of Fig. 4a, b), respectively. Both analogues, sharing the identical core structure with TGlu, demonstrated consistent performance with TGlu in solution, solid and film state, all exhibiting approximately a quantum yield 90% (Fig. 4a, b). Also, they show consistent emission properties minimally dependent on the solvent polarity and viscosity (see Supplementary Figs. 21 and 22 and Table 5 for EH-TGlu and Supplmentary Figs. 23 and 24 and Table 6 for EG-TGlu in detail). This confirmed that the fluorescence properties of TGlu remain stable even when different alkoxy groups are tethered.

https://doi.org/10.1038/s41467-025-60316-0

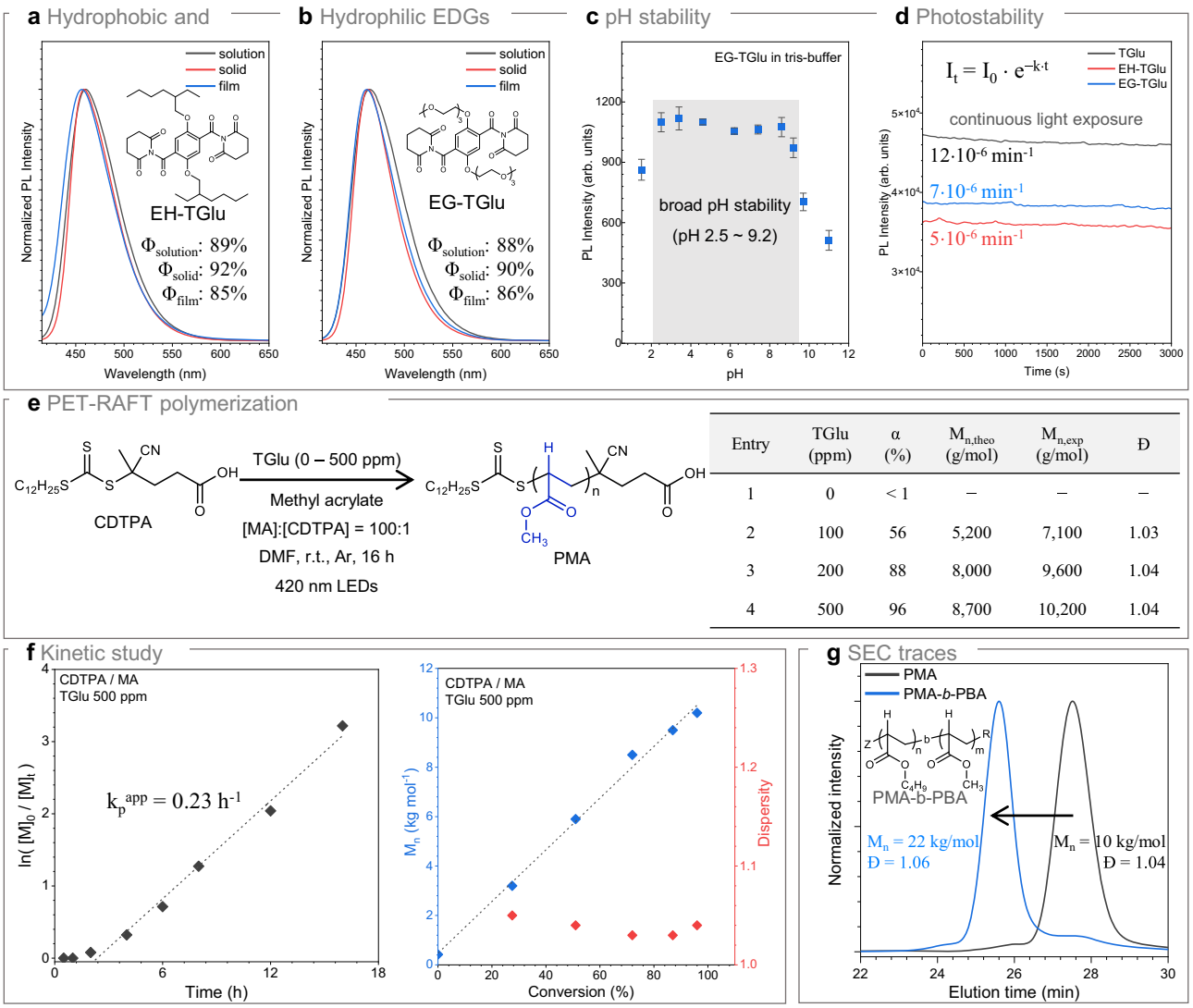

Entry	TGlu (ppm)	α (%)	$M_{n,theo}$ (g/mol)	$M_{n,exp}$ (g/mol)	Đ
1	0	< 1	–	–	–
2	100	56	5,200	7,100	1.03
3	200	88	8,000	9,600	1.04
4	500	96	8,700	10,200	1.04

Fig. 4 | Photophysical properties, stability, and PET-RAFT polymerisation. Emission spectra of EH-TGlu (**a**) and EG-TGlu (**b**) in solution, solid, and film states. **c** pH stability ranging from 1 to 12; three freshly prepared samples were measured to estimate error bars. **d** Photostability under continuous light exposure for 50 min. **e** PET-RAFT polymerisation using TGlu as a photocatalyst with CDPTA and MA, with a summarised table of results. Supplementary Fig. 30 shows SEC trace profiles of the polymerisations process. **f** Kinetic study showing the relationship between monomer conversion and light exposure time (left), and between molecular weight and conversion (right), indicating the living nature of the resulting polymers. **g** SEC traces demonstrate block-copolymerisation without any purification.

In addition, to further evaluate the stability of TGlu, we investigated the pH stability and photostability of these fluorophores before utilising TGlu in both solution and solid-phase applications (Fig. 4c, d, respectively). As shown in Fig. 4c, EG-TGlu in tris buffer exhibits a broad pH stability window from 2.5 to 9.2, with a hypsochromic shift observed at higher pH levels, around 10 (Supplementary Fig. 25)[1].H-NMR spectra indicate hydrolysis of the amide group (Supplementary Fig. 26). Also, the emission remains stable under continuous light exposure at the absorption maximum of 395 nm, with a slow degradation rate constant (k) of approximately $8 \times 10^{-6}\,min^{-1}$ (Fig. 4d)[77].

PET-RAFT polymerisation

Given TGlu's exceptional photostability and high Φ_F, its largely stabilised LUMO, its potential as a photocatalyst (PC) for photoinduced electron/energy transfer reversible addition–fragmentation chain transfer (PET-RAFT) polymerisation was investigated[78]. PET-RAFT polymerisation utilises thiocarbonylthio compounds to facilitate degenerative chain transfer, with PCs serving as sources of energy and/or electron transfer for radical generation[79,80]. In this study, methyl acrylate (MA) was selected as the monomer, 4-cyano-4-[(dodecylsulfanylthiocarbonyl)sulfanyl]pentanoic acid (CDPTA) as the RAFT agent, following established PET-RAFT methodologies. The ground-state redox potentials against the saturated calomel electrode (SCE) were then estimated. The photophysical and electrochemical properties of TGlu ($E_{ox}^* = -1.06$ V versus SCE; $E_{00}(S_1) = 2.84$ eV) suggest that it possesses the requisite values for effective electron/energy transfer to CDPTA (Supplementary Fig. 27)[81]. A 420 nm LED light source was employed to facilitate the excitation of TGlu (Supplementary Fig. 28).

In a control experiment, polymerisation was attempted under inert conditions for 16 h via a photoiniferter process without the addition of a PC, which resulted in no observable polymerisation (Fig. 4e – ***entry 1***). This outcome is likely due to the inefficient overlap between the 420 nm light source and the nπ* absorption region of CDPTA[82]. The subsequent addition of 100 ppm TGlu led to a monomer conversion (α) of 56%, with a narrow molecular weight dispersity ($M_n = 7100$ g/mol, Đ = 1.03) as measured by size exclusion

chromatography (SEC) with a refractive index detector, indicating TGlu's effectiveness as a PC in the PET-RAFT process (Fig. 4e – *entry 2*). A further increase in TGlu concentration to 500 ppm resulted in an enhanced conversion while maintaining narrow dispersity (Fig. 4e – *entries 3–4*). The living nature of the resulting polymers was confirmed via ^{1}H NMR, which demonstrated the retention of the trithiocarbonate functional group (3.32–3.39 ppm), indicating high end-group fidelity (Supplementary Fig. 29). In addition, a linear relationship was observed between monomer conversion and both light exposure time and molecular weight (Fig. 4f). Without additional purification, block-copolymerisation with n-butyl acrylate was successfully carried out, yielding a distinct shift in the SEC trace while preserving narrow dispersity (Đ = 1.06; Fig. 4g). In-situ thin layer chromatography (TLC) analysis further confirmed that TGlu remained highly stable throughout the 24 h PET-RAFT polymerisation process (Supplementary Fig. 31). These results demonstrate the highly effective performance of TGlu as a PC in the PET-RAFT polymerisation system.

It is important to note, however, that the high Φ_F of TGlu, while notable, is not the primary factor driving its photocatalytic efficiency. Instead, the efficiency of PET-RAFT polymerisation is primarily governed by electron transfer dynamics in the photo-excited state. Comparative studies (Supplementary Figs. 32, 33 for TSuc, TPid, respectively) demonstrate that TGlu surpasses other SBFs in photocatalytic efficiency due to its well-balanced photophysical properties, which include an optimal excited-state lifetime and redox potential, rather than its high emission efficiency alone.

Optical waveguiding

High quantum yield with stable emission in optical waveguiding materials leads to stronger, more efficient, and longer-lasting light propagation with low loss[83,84]. To achieve minimum defects and eliminate grain boundaries, which is critical for reducing the light-scattering loss, we investigated the TGlu single crystals for this purpose. The well-defined one-dimensional crystal shows bright edge-emission upon bulk excitation, indicating the potential of TGlu as an excellent optical waveguiding material (Fig. 5a). The crystal exhibited intense fluorescence at 464 nm, a relatively low quantum yield of 54%, and a lifetime of 6.3 ns (Fig. 5b, c).

To accurately evaluate waveguide efficiency, we assessed the intensity of light emitted from the tip using spatially resolved emission spectra of an individual crystal with a focused laser. As shown in Fig. 5d, we observed efficient optical waveguiding properties with low propagation losses (α = 6.1 dB/mm).

Discussion

In this study, we successfully designed a novel single benzene fluorophore (SBF), namely TGlu, which achieves high quantum yields, reaching close-to-unity blue fluorescence efficiency in both solution and solid phases. The design concept was based on the common SBF double ortho-donor-acceptor quadrupole motif, but with an inventive new D-A pairing, utilising sterically demanding acceptor moieties, with the rationale to suppress both nonradiative decay in solution and the solid state; this could be indeed fully confirmed. Systematic studies on structural analogues elucidated the reason for the suppressed nonradiative decay in solution, exhibiting an 'inverted energy gap law behaviour' due to thermodynamic control on the access to the conical intersection. Finally, the versatility of TGlu was demonstrated in various applications: as a highly effective photocatalyst for PET-RAFT polymerisation in solution, and as an efficient optical waveguide in its single-crystal form, exhibiting low propagation losses. Overall, this study provides valuable insights into the targeted design of small-size high-efficiency organic fluorophores with potential applications in both solution and solid phases, simplifying the design and selection process for practical applications.

Methods

Optical spectroscopy

To study the optical properties of inverstigated chromophores (e.g., TGlu, TSuc, TPid, TPip, EH-TGlu, EG-TGlu), samples were preprated in spectroscopic grade solvents (Aldrich Chemical Co.) at a concentration of 1×10^{-5} M. The optical properties of the samples were studied through UV-visible absorption spectra, recorded on a Varian Cary50 UV/Vis spectrophotometer. Photoluminescence attributes, absolute quantum yield, and time-resolved fluorescence lifetime were measured using a Photon Technologies International (PTI) QuantaMaster TM spectrofluorometer. UV–visible absorption spectra were recorded with a Varian Cary 50 spectrophotometer. Photoluminescence (PL) emission spectra of both solutions and crystals were collected on a Photon Technologies International (PTI) QuantaMaster spectrofluorometer (QM-400), equipped with a continuous 75 W Xe lamp. Emission was detected at a 90° angle using a Horiba PMT-928 photomultiplier tube; the spectra were corrected for the λ-dependence of the detector. For solid-state measurements, crystals were placed in Wilmad quartz NMR tubes (Aldrich Chemical Co.) on a quartz mount. Low-temperature measurements were carried out by immersing the quartz mount in liquid nitrogen. Fluorescence lifetime measurements were conducted using a time-correlated single photon counting (TCSPC) technique attached to the spectrometer, equipped with a DD-C1 picosecond diode controller, a DH-HT high-throughput TCSPC controller, and a DeltaDiode (DD-425L) LED light source emitting at 421 nm. Mono-exponential (or bi-exponential) decay fitting was performed using FelixGX software to determine the fluorescence lifetimes. PL quantum yields were determined using a calibrated integrating sphere attached to the spectrometer, with data measured against a blank sample. Each measurement was performed four times on freshly prepared samples to ensure consistency. All measurements showed high repeatability, and errors are reported as ±1 standard deviation. To verify measurement reliability, rhodamine 6 G (R6G) and coumarin 153 were studied as reference dyes following standard literature protocols[85].

Structural analysis

Powder X-ray diffraction (PXRD) patterns were recorded using a PANalytical Empyrean diffractometer in Bragg–Brentano geometry with Cu Kα radiation, operating at 45 kV and 40 mA. The incident beam was configured with a Bragg–BrentanoHD X-ray optic and fixed/soller slits. X-ray detection was performed using a silicon-based linear position-sensitive X'Celerator Scientific detector in 1D scanning mode. PXRD data were collected over a 2θ range of 3–50° with a scan rate of 0.00835° per step.

Single-crystal X-ray diffraction data were collected using a Rigaku XtaLAB Synergy-S X-ray diffractometer with a kappa goniometer geometry configuration. The X-ray source is a PhotonJet-S microfocus Cu source (λ = 1.54184 Å) operated at 50 kV and 1 mA. X-ray intensities were measured with a HyPix-6000HE detector held 34 mm from the sample. The data were processed using CrysAlisPro v40.82 (Rigaku Oxford Diffraction) and were corrected for absorption. The structures were determined and refined using OLEX2[86] v1.5-ac5-024 with SHELXT[87] and SHELXL[88]. All non-hydrogen atoms were refined anisotropically with hydrogen atoms located in idealised positions. Deposition Number 2376729 contains the supplementary crystallographic data for TGlu.

Quantum-chemical calculations

Ground- and excited-state geometry optimisations were performed in vacuum using (time-dependent) density functional theory ((TD-)DFT); for the symmetrical molecules, the optimisation was done in the point group C_2. Energy minima were confirmed by the absence of imaginary frequencies in the harmonic vibrational analysis. Rigid scans were performed by fixing the torsional angle (θ, φ) to certain values,

https://doi.org/10.1038/s41467-025-60316-0

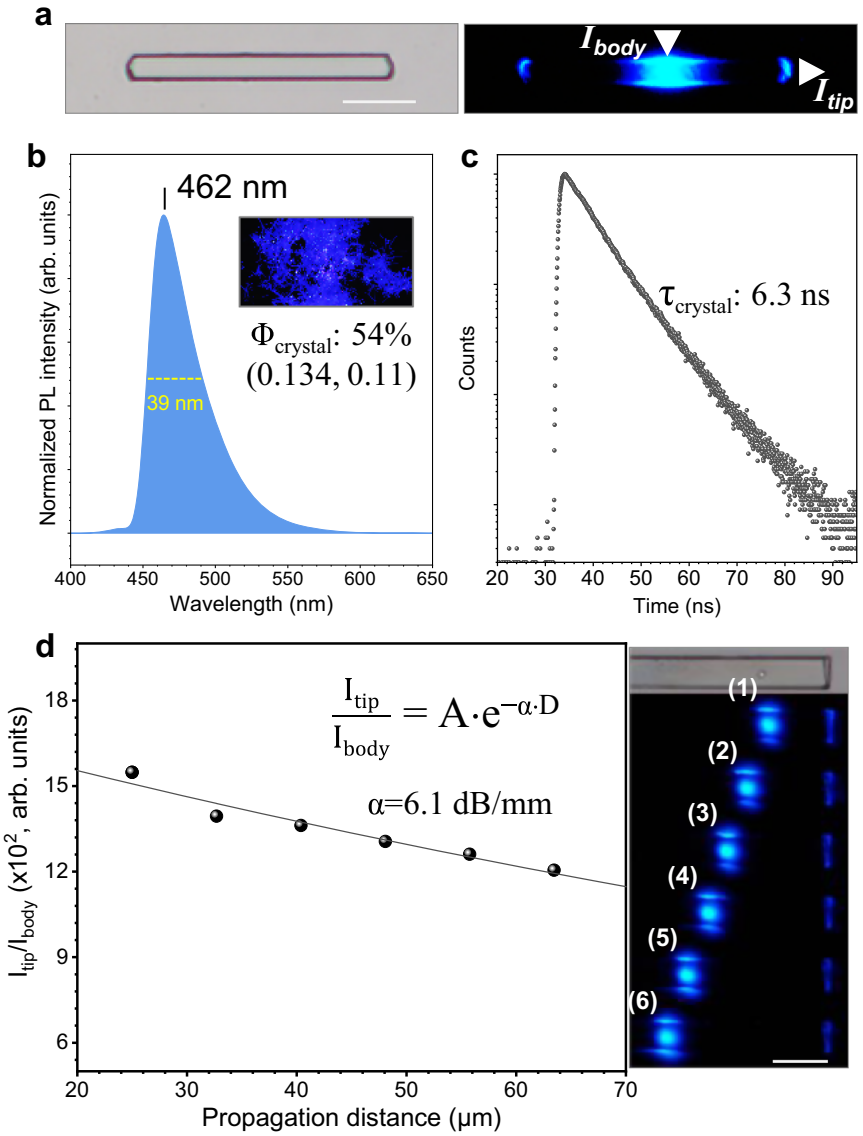

Fig. 5 | Optical waveguiding in 1-D single crystal of TGlu. a Optical microscope images of a 1-D single crystal of TGlu with bright field (left) and focal excitation at body (right). Emission (**b**) and lifetime decay (**c**) spectra of the crystal. **d** Intrinsic loss coefficient measured from the plot of propagation distance-dependent relative tip emission intensity (scale bar = 100 μm in **a**, **d**).

running single-point calculations on these geometries. MO topologies were plotted with ChemCraft, using a contour value of 0.02. For the optical properties, all calculations were performed at the time-dependent DFT (TD-DFT) level in vacuum and in DCM. For all cases, the B3LYP functional (6-311 G(d) basis set) was applied, as implemented in Gaussian 16 programme[89] Solvent effects were described using a polarisable continuum model (PCM)[90]. system due to the consideration of the dispersion correlation. For TGlu-DMSO optimisation, the S-$O_{carbonyl}$ distance was fixed to the van-der-Waals distance (3.3 Å), and the D3-B3LYP functional was used to account for dispersion effects.

Vibronically resolved spectra were calculated using FCclasses3, including thermal population at 298 K[91]; here, geometries and vibrational modes were obtained by the D3-B3LYP functional for the optimised geometries and vibrations in S0 and S1, which was found to perform well for the spectral position and band shapes. To display the spectra in the wavelength scale, the calculated emission spectrum was divided by λ^2. Gaussian broadening with a width of γG = 0.07 eV was applied in all cases to compare with the experiment.

In order to explore the path towards the conical intersection, the excited-state transition state was optimised at the TD-DFT level only, for which analytical second derivatives of the energy with respect to nuclear coordinates could be computed. The mixed-reference spin-flip TD-DFT (MR-SF-TD-DFT) method[92] was used to locate conical intersections, as it allows a correct description of the potential energy surface topology where the ground- and first excited state couple[93]. All the MR-SF-TD-DFT calculations were performed with the recommended restricted open-shell BHHLYP functional[94] and the 6-31 G(d) basis set using GAMESS[95]. MO topologies were plotted with ChemCraft, using a contour value of 0.02.

PET-RAFT Polymerisation

A typical PET-RAFT procedure for the reaction with a monomer-to-RAFT agent ratio of [MA]:[CDTPA] = [100]:[1] was conducted as follows. The inhibitor in methyl acrylate (MA) was removed by passing it through a basic aluminium oxide column. A stock solution of **TGlu** was prepared at a concentration of 10 mg/mL in anhydrous DMF. A 20 mL glass vial, equipped with a stirring bar, was charged with MA (1.0 mL, 11.1 mmol), CDTPA (45.0 mg, 1.11·10-1 mmol), TGlu stock solution

(0.22 mL (2.2 mg), $5.55{\cdot}10^{-3}$ mmol for 500 ppm) and an additional 0.78 mL of anhydrous DMF as the solvent. The vial was then capped with a rubber septum, sealed with parafilm, and purged with argon (99.99%) for 30 min. Polymerisation was subsequently performed under 420 nm LEDs at room temperature. After the polymerisation process, a 0.2 mL aliquot of the reaction mixture was removed using a syringe. The aliquot was split, with 0.1 mL dissolved in $CDCl_3$ and 0.1 mL in THF. These samples were immediately analysed without storage[1]:H NMR was used for conversion and end-group analysis, SEC for molecular weight (MW) and dispersity (Đ) analysis. The molecular weights (MWs) and molecular weight distributions of the synthesised polymers were determined using size exclusion chromatography (SEC) with a Waters 1515 isocratic HPLC pump, coupled to a refractive index (RI) detector (Waters 2414). The analysis was performed with three Styragel columns (HR 1, HR 3, HR 4, Waters) using tetrahydrofuran as the eluent at 35 °C and a flow rate of 0.8 mL/min. Polystyrene standards were employed for calibration.

Optical waveguiding

The optical properties of the TGlu crystal, including colour charge-coupled device (CCD) imaging and fluorescence spectroscopy, were measured using a custom-built laser confocal microscope (LCM) system with high spatial resolution (≤ 200 nm). To accurately characterise planar optical waveguiding effects, the LCM system was modified to separate the positions of the incident laser from those of the detector. The precise positioning of the incident laser was achieved using a piezoelectric 2D positioning system (Albatross, Nanofocus Inc.). The excitation wavelength (λ_{ex}) was set to 395 nm for both luminescent colour CCD imaging and fluorescence spectra acquisition, recorded using a GF-033C-IRF (Allied Vision) and an SR-303I-B (Andor), respectively.

Data availability

The data supporting the findings of this study are available in the Supplementary Information. Source data for the main figures are provided in a separate Source Data file. All electronic structure files are included in Supplementary Data 1. Additional data supporting the Supplementary Information are available from the corresponding authors upon request. Source data are provided in this paper.

References

1. Wolfbeis, O. S. An overview of nanoparticles commonly used in fluorescent bioimaging. *Chem. Soc. Rev.* **44**, 4743–4768 (2015).
2. Li, W., Kaminski Schierle, G. S., Lei, B., Liu, Y. & Kaminski, C. F. Fluorescent nanoparticles for super-resolution imaging. *Chem. Rev.* **122**, 12495–12543 (2022).
3. Singh, V. K. et al. Highly efficient organic photocatalysts discovered via a computer-aided-design strategy for visible-light-driven atom transfer radical polymerization. *Nat. Catal.* **1**, 794–804 (2018).
4. Marzo, L., Pagire, S. K., Reiser, O. & König, B. Visible-light photocatalysis: does it make a difference in organic synthesis?. *Angew. Chem. Int. Ed.* **57**, 10034–10072 (2018).
5. Adachi, C., Hattori, R. & Kaji, H. in *Handbook of Organic Light-Emitting Diodes*. (ed. Tsujimura, T.) (Springer, Tokyo, Japan, 2020).
6. Jiang, Y. et al. Organic solid-state lasers: A materials view and future development. *Chem. Soc. Rev.* **49**, 5885–5944 (2020).
7. Gierschner, J., Varghese, S. & Park, S. Y. Organic single crystal lasers: a materials view. *Adv. Opt. Mater.* **4**, 348–364 (2016).
8. Wang, X., Wolfbeis, O. S. & Meier, R. J. Luminescent probes and sensors for temperature. *Chem. Soc. Rev.* **42**, 7834–7869 (2013).
9. Velema, W. A., Szymanski, W. & Feringa, B. L. Photopharmacology: beyond proof of principle. *J. Am. Chem. Soc.* **136**, 2178–2191 (2014).
10. Yan, D. & Evans, D. G. Molecular crystalline materials with tunable luminescent properties: from polymorphs to multi-component solids. *Mater. Horiz.* **1**, 46–57 (2014).
11. Carella, A., Borbone, F. & Centore, R. Research progress on photosensitizers for DSSC. *Front. Chem.* **6**, 481 (2018).
12. Gierschner, J. et al. Luminescence in crystalline organic materials: from molecules to molecular solids. *Adv. Opt. Mater.* **9**, 2002251 (2021).
13. Würthner, F. Aggregation-induced emission (AIE): a historical perspective. *Angew. Chem. Int. Ed.* **59**, 14192–14196 (2020).
14. Stenspil, S. G. & Laursen, B. W. Photophysics of fluorescent nanoparticles based on organic dyes – challenges and design principles. *Chem. Sci.* **15**, 8625–8638 (2024).
15. Rodríguez-Cortés, L. A. et al. Conformational emissive states in dual-state emitters with benzotriazole acceptors. *Matter* **6**, 1140–1159 (2023).
16. Huber, A., Dubbert, J., Scherz, T. D. & Voskuhl, J. Design concepts for solution and solid-state emitters–a modern viewpoint on classical and non-classical approaches. *Chem. Eur. J.* **29**, e202202481 (2023).
17. Gierschner, J., Lüer, L., Milián-Medina, B., Oelkrug, D. & Egelhaaf, H. J. Highly emissive H-aggregates or aggregation-induced emission quenching? The photophysics of all-trans para-distyrylbenzene. *J. Phys. Chem. Lett.* **4**, 2686–2697 (2013).
18. Huang, Y. et al. Competition between triplet pair formation and excimer-like recombination controls singlet fission yield. *Cell Rep. Phys. Sci.* **2**, 100339 (2021).
19. Oelkrug, D. et al. Tuning of fluorescence in films and nanoparticles of oligophenylenevinylenes. *J. Phys. Chem. B* **102**, 1902–1907 (1998).
20. Shi, J. et al. Solid state luminescence enhancement in π-conjugated materials: unraveling the mechanism beyond the framework of AIE/AIEE. *J. Phys. Chem. C.* **121**, 23166–23183 (2017).
21. Gierschner, J. & Park, S. Y. Luminescent distyrylbenzenes: tailoring molecular structure and crystalline morphology. *J. Mater. Chem. C.* **1**, 5818–5832 (2013).
22. Barbara, P. F., Rand, S. D. & Rentzepis, P. M. Direct measurements of tetraphenylethylene torsional motion by picosecond spectroscopy. *J. Am. Chem. Soc.* **103**, 2156–2162 (1981).
23. Prlj, A., Doslic, N. & Corminboeuf, C. How does tetraphenylethylene relax from its excited states?. *Phys. Chem. Chem. Phys.* **18**, 11606–11609 (2016).
24. Crespo-Otero, R., Li, Q. & Blancafort, L. Exploring potential energy surfaces for aggregation-induced emission—from solution to crystal. *Chem. Asian J.* **14**, 700–714 (2019).
25. Peng, X.-L., Ruiz-Barragan, S., Li, Z.-S., Li, Q.-S. & Blancafort, L. Restricted access to a conical intersection to explain aggregation induced emission in dimethyl tetraphenylsilole. *J. Mater. Chem. C.* **4**, 2802–2810 (2016).
26. Behera, S. K., Park, S. Y. & Gierschner, J. Dual emission: classes, mechanisms, and conditions. *Angew. Chem. Int. Ed.* **60**, 22624–22638 (2021).
27. Huber, A., Dubbert, J., Scherz, T. D. & Voskuhl, J. Design concepts for solution and solid-state emitters – A modern viewpoint on classical and non-classical approaches. *Chem. Eur. J.* **29**, e202202481 (2023).
28. Shimizu, M., Takeda, Y., Higashi, M. & Hiyama, T. 1, 4-Bis (alkenyl)-2, 5-dipiperidinobenzenes: Minimal Fluorophores Exhibiting Highly Efficient Emission in the Solid State. *Angew. Chem. Int. Ed.* **48**, 3653–3656 (2009).
29. Tang, B., Wang, C., Wang, Y. & Zhang, H. Efficient red-emissive organic crystals with amplified spontaneous emissions based on a single benzene framework. *Angew. Chem. Int. Ed.* **56**, 12543–12547 (2017).
30. Kim, J., Oh, J. H. & Kim, D. Recent advances in single-benzene-based fluorophores: Physicochemical properties and applications. *Org. Biomol. Chem.* **19**, 933–946 (2021).
31. Xiang, Z. et al. A general strategy for development of a single benzene fluorophore with full-color-tunable, environmentally

insensitive, and two-photon solid-state emission. *Chem. Commun.* **55**, 11462–11465 (2019).
32. Okada, Y., Sugai, M. & Chiba, K. Hydrogen-bonding-induced fluorescence: water-soluble and polarity-independent solvatochromic fluorophores. *J. Org. Chem.* **81**, 10922–10929 (2016).
33. Sarkar, S. et al. Interactive twin intramolecular hydrogen bonds enable bright, S-Blue emissive, environment-insensitive single-benzene fluorophores. *Adv. Funct. Mater.* **33**, 2304507 (2023).
34. Kim, H., Kim, Y. & Lee, D. Small is beautiful: electronic origin and synthetic evolution of single-benzene fluorophores. *Acc. Chem. Res.* **57**, 140–152 (2024).
35. Kim, H. et al. Relief of excited-state antiaromaticity enables the smallest red emitter. *Nat. Commun.* **12**, 5409 (2021).
36. Huang, R., Liu, B., Wang, C., Wang, Y. & Zhang, H. Constructing full-color highly emissive organic solids based on an X-shaped tetra-substituted benzene skeleton. *J. Phys. Chem. C.* **122**, 10510–10518 (2018).
37. Beppu, T., Tomiguchi, K., Masuhara, A., Pu, Y.-J. & Katagiri, H. Single benzene green fluorophore: solid-state emissive, water-soluble, and solvent-and pH-independent fluorescence with large Stokes shifts. *Angew. Chem. Int. Ed.* **54**, 7332–7335 (2015).
38. Bao, Z. et al. Single-benzene fluorophores: Controlling electron density on amino of 2, 5-diaminoterephthalates to manipulate optical/electronic properties for efficient and diversified functions. *Adv. Funct. Mater.* **34**, 2403954 (2024).
39. Cho, E. et al. A single-benzene-based fluorophore: Optical waveguiding in the crystal form. *ChemPlusChem* **84**, 1130–1134 (2019).
40. Jin, J. H.et aL. Amino-SBBF (Single Benzene-based Fluorophore) library: Its synthesis, photophysical property, and cellular imaging application. *Dyes Pigm* **221**, 111811 (2024).
41. Kim, Y. et al. Single-benzene dual-emitters harness excited-state antiaromaticity for white light generation and fluorescence imaging. *Angew. Chem. Int. Ed.* **62**, e202302107 (2023).
42. Jung, Y. et al. Development of a fluorescent nanoprobe based on an amphiphilic single-benzene-based fluorophore for lipid droplet detection and its practical applications. *Org. Biomol. Chem.* **20**, 5423–5433 (2022).
43. Kim, D. et al. Structural and electronic tuning of single-benzene fluorophores with simple methylations. *Dyes Pigm.* **233**, 112523 (2025).
44. Raghava, T., Banerjee, S. & Chattopadhyay, A. Diamino-terephthalonitrile-based single benzene fluorophores featuring strong solution state fluorescence and large Stokes shifts. *J. Org. Chem.* **88**, 15708–15716 (2023).
45. Raghava, T., Chattopadhyay, A., Bhavana, P. & Banerjee, S. Amino-terephthalonitrile-based single benzene fluorophores with large stokes shifts and solvatochromic behavior. *Chem. Asian J.* **18**, e202201314 (2023).
46. Zhang, X. et al. Efficient single benzene AIE system: Optical waveguide and invisible ink. *Dyes Pigm* **209**, 110947 (2023).
47. Coehlo, M., Thuéry, P. & Pieters, G. Chiral perturbation on single benzene-based fluorophores: A structure/(chir) optical activity relationship study. *Chirality* **35**, 796–804 (2023).
48. Cao, H. et al. Tuning molecular packing by twisting structure to facilely construct highly efficient solid-state fluorophores for two-photon bioimaging and photodynamic therapy. *Adv. Funct. Mater.* **34**, 2315692 (2024).
49. Mandal, M. et al. Innovative strategy toward red emission: single-benzenic, ultrasmall meta-fluorophores. *J. Phys. Chem. C.* **124**, 27049–27054 (2020).
50. Zhang, J. N. et al. Organic solid fluorophores regulated by subtle structure modification: color-tunable and aggregation-induced emission. *Chem. Sci.* **8**, 577–582 (2017).
51. Göbel, D., Duvinage, D., Stauch, T. & Nachtsheim, B. J. Nitrile-substituted 2-(oxazolinyl)-phenols: minimalistic excited-state intramolecular proton transfer (ESIPT)-based fluorophores. *J. Mater. Chem. C.* **8**, 9213–9225 (2020).
52. Tang, B., Liu, H., Li, F., Wang, Y. & Zhang, H. Single-benzene solid emitters with lasing properties based on aggregation-induced emissions. *Chem. Commun.* **52**, 6577–6580 (2016).
53. Raghava, T., Chattopadhyay, A., Banerjee, S. & Sarkar, N. Conversion of amino-terephthalonitriles to multi-substituted single benzene fluorophores with utility in bioimaging. *Org. Biomol. Chem.* **22**, 364–373 (2024).
54. Grabowski, Z. R., Rotkiewicz, K. & Rettig, W. Structural changes accompanying intramolecular electron transfer: focus on twisted intramolecular charge-transfer states and structures. *Chem. Rev.* **103**, 3899–4032 (2003).
55. Baeyer, A. Ueber den Succinylobernsteinsäureäther. *Ber. Dtsch. Chem. Ges.* **19**, 428–433 (1886).
56. Hojo, N. & Yoneno, H. Preparation of 2,5-diaminoterephthalic acid by the Hofmann degradation of pyromellitic di-imide (benzene-1,2,4,5-tetracarboxylic 1,2:4,5-di-imide) in the presence of metal salts. *J. Chem. Soc. A* **2387**, 2389 (1970).
57. Shimizu, M. et al. 1, 4-Bis (diarylamino)-2, 5-bis (4-cyanophenylethenyl) benzenes: Fluorophores Exhibiting Efficient Red and Near-Infrared Emissions in Solid State. *Angew. Chem. Int. Ed.* **51**, 4095–4099 (2012).
58. Kim, M. A., Whang, D. R., Gierschner, J. & Park, S. Y. A distyrylbenzene based highly efficient deep red/near-infrared emitting organic solid. *J. Mater. Chem. C.* **3**, 231–234 (2015).
59. Terenziani, F., Painelli, A., Katan, C., Charlot, M. & Blanchard-Desce, M. Charge instability in quadrupolar chromophores: Symmetry breaking and solvatochromism. *J. Am. Chem. Soc.* **128**, 15742–15755 (2006).
60. Grinter, R. & Heilbronner, E. Energie und Ladungsverteilung von elektronisch angeregten Zuständen mehrfach substituierter Benzole: Eine quantenchemische Deutung der Witt-Dilthey-Wizinger'schen Farbregeln. *Helv. Chim. Acta* **45**, 2496–2516 (1962).
61. Griffiths, J. Recent developments in the colour and constitution of organic dyes. Review of progress in coloration and related topics. *Rev. Prog. Color. Relat. Top.* **11**, 37–57 (1981).
62. Shi, J. et al. Inverted energy gap law for the nonradiative decay in fluorescent floppy molecules: larger fluorescence quantum yields for smaller energy gaps. *Org. Chem. Front.* **6**, 1948–1954 (2019).
63. Izquierdo, M. A. et al. Excited-state non-radiative decay in stilbenoid compounds: an ab initio quantum-chemistry study on size and substituent effects. *Phys. Chem. Chem. Phys.* **21**, 22429–22439 (2019).
64. Hoche, J. et al. The origin of the solvent dependence of fluorescence quantum yields in dipolar merocyanine dyes. *Chem. Sci.* **10**, 11013–11022 (2019).
65. Feng, Y. et al. Fluorescence modulation through the inverted energy gap law in triply N–B←N-containing windmill-shaped triazines. *Angew. Chem. Int. Ed.* **64**, e202416425 (2025).
66. Barneschi, L. et al. On the fluorescence enhancement of arch neuronal optogenetic reporters. *Nat. Commun.* **13**, 6432 (2022).
67. Reichardt, C. & Welton, T. *Solvents and Solvent Effects in Organic Chemistry*. (John Wiley & Sons, 2011).
68. Gierschner, J., Mack, H.-G., Lüer, L. & Oelkrug, D. Fluorescence and absorption spectra of oligophenylenevinylenes: Vibronic coupling, band shapes, and solvatochromism. *J. Chem. Phys.* **116**, 8596–8609 (2002).
69. Milián Medina, B. et al. EDOT-type materials: planar but not rigid. *J. Phys. Chem. A* **112**, 13282–13286 (2008).
70. Griffiths, J., Lockwood, M. & Roozpeik, B. Orientation effects in the benzene chromophore bearing one donor and two acceptor groups. Electronic absorption spectra of the dicyanoanilines. *J. Chem. Soc. Perkin Trans.* **2**, 1608–1610 (1977).

71. Gierschner, J., Cornil, J. & Egelhaaf, H.-J. Optical bandgaps of π-conjugated organic materials at the polymer limit: experiment and theory. *Adv. Mater.* **19**, 173–191 (2007).
72. Englman, R. & Jortner, J. The energy gap law for radiationless transitions in large molecules. *Mol. Phys.* **18**, 145–164 (1970).
73. Song, S. et al. J. Rational design of color-pure blue organic emitters by poly-heteroaromatic omni-delocalization. *Adv. Mater.* **33**, 2404388 (2024).
74. Eskandari, M., Wang, L., Milián-Medina, B. & Gierschner, J. Paper and pencil design of color-Pure organic emitters: The curious case of xanthene dyes. *J. Phys. Chem. A* **129**, 1599–1608 (2025).
75. Srinivasan, G. et al. Dynamics of guest molecules in PHTP inclusion compounds as probed by solid-state NMR and fluorescence spectroscopy. *Phys. Chem. Chem. Phys.* **11**, 4996–5009 (2009).
76. Cerezo, J., Gierschner, J., Santoro, F. & Prampolini, G. Explicit modelling of spectral bandshapes by a mixed quantum-classical approach: Solvent order and temperature effects in the optical spectra of distryrylbenzene. *ChemPhysChem* **25**, e202400307 (2024).
77. Demchenko, A. P. Photobleaching of organic fluorophores: quantitative characterization, mechanisms, protection. *Methods Appl. Fluoresc.* **8**, 022001 (2020).
78. Xu, J., Jung, K., Atme, A., Shanmugam, S. & Boyer, C. A robust and versatile photoinduced living polymerization of conjugated and unconjugated monomers and its oxygen tolerance. *J. Am. Chem. Soc.* **136**, 5508–5519 (2014).
79. Corrigan, N. et al. Reversible-deactivation radical polymerization (Controlled/living radical polymerization): From discovery to materials design and applications. *Prog. Polym. Sci.* **111**, 101311 (2020).
80. Lee, Y., Boyer, C. & Kwon, M. S. Photocontrolled RAFT polymerizati on: past, present, and future. *Chem. Soc. Rev.* **52**, 3035–3097 (2023).
81. Yu, C. et al. Silver sulfide nanocrystals as a biocompatible and full-spectrum photocatalyst for efficient light-driven polymerization under aqueous and ambient conditions. *ACS Catal.* **13**, 665–680 (2022).
82. Hughes, R. W., Lott, M. E., Bowman, J. I. & Sumerlin, B. S. Excitation dependence in photoiniferter polymerization. *ACS Macro Lett.* **12**, 14–19 (2023).
83. Wu, S., Zhou, B. & Yan, D. Recent advances on molecular crystalline luminescent materials for optical waveguides. *Adv. Opt. Mater.* **9**, 2001768 (2021).
84. Liu, F. et al. Light-emitting metal–organic halide 1D and 2D structures: Near-unity quantum efficiency, low-loss optical waveguide and highly polarized emission. *Angew. Chem. Int. Ed.* **60**, 13548–13553 (2021).
85. Würth, C., Grabolle, M., Pauli, J., Spieles, M. & Resch-Genger, U. Relative and absolute determination of fluorescence quantum yields of transparent samples. *Nat. Protoc.* **8**, 1535–1550 (2013).
86. Dolomanov, O. V., Bourhis, L. J., Gildea, R. J., Howard, J. A. & Puschmann, H. OLEX2: a complete structure solution, refinement and analysis program. *J. Appl. Crystallogr.* **42**, 339–341 (2009).
87. Sheldrick, G. M. SHELXT–Integrated space-group and crystal-structure determination. *Acta Cryst. A* **71**, 3–8 (2015).
88. Sheldrick, G. M. Crystal structure refinement with SHELXL. *Acta Cryst. C.* **71**, 3–8 (2015).
89. Frisch, M. J. et al. Gaussian 16 Rev. C.01; Gaussian Inc.: Wallingford, CT, (2016).
90. Cerezo, J. & Santoro, F. FCclasses3: Vibrationally-resolved spectra simulated at the edge of the harmonic approximation. *J. Comput. Chem.* **44**, 626–643 (2023).
91. Tomasi, J., Mennucci, B. & Cammi, R. Quantum mechanical continuum solvation models. *Chem. Rev.* **105**, 2999–3094 (2005).
92. Lee, S., Filatov, M., Lee, S. & Choi, C. H. Eliminating spin-contamination of spin-flip time dependent density functional theory within linear response formalism by the use of zeroth-order mixed-reference (MR) reduced density matrix. *J. Chem. Phys.* **149**, 104101 (2018).
93. Minezawa, N. & Gordon, M. S. Optimizing conical intersections by spin– flip density functional theory: application to ethylene. *J. Phys. Chem. A* **113**, 12749–12753 (2009).
94. Becke, A. D. A new mixing of Hartree-Fock and local density-functional theories. *J. Chem. Phys.* **98**, 1372–1377 (1993).
95. Schmidt, M. W. et al. General atomic and molecular electronic structure system. *J. Comput. Chem.* **14**, 1347–1363 (1993).

Acknowledgements

This work was financially supported by KLA-Tencor Corporation and the National Research Foundation of Korea (NRF) grant funded by the Korea government (MSIT)(No. RS-2021-NR060082). The work in Madrid was supported by the Spanish Science Ministry (MICN-FEDER PID2022-138222NB-C21), the 'Severo Ochoa' programme (MINECO SEV-2016-0686), and the Campus of International Excellence UAM + CSIC. The work in Valencia was supported by MICN-FEDER (PID2022-138222NB-C22, RED2022-134503-T). The work in Tübingen acknowledges regional funding from Baden-Württemberg via bwHPC, and from the DFG (INST 40/575-1 FUGG, JUSTUS 2 cluster). The work at SNU was partially supported by the SNU OPEN WORLD international collaborative research programme. M.F.F.-A. acknowledges the IDEAL PhD training programme, co-funded by the EU and Comunidad Madrid (H2020-MSCA-COFUND-2020; agreement 101034431). C.Y. acknowledges support from the BK21 FOUR project and the SNU overseas training programme. H.W. and A.J.M. acknowledge support from the U.S. Department of Energy BES (Grant DE-SC0004888) for structural analyses.

Author contributions

J.-M.H., M.S.K., J.G. and J.K. conceived and supervised the project. J.-M.H. and J.P. synthesised and characterised the investigated compounds. The photophysical pathways were analysed by J.-M.H., J.P. and J.G. The (TD-)DFT calculations were conducted and analysed by M.F.F.-A. and the MR-SF-TD-DFT calculations by L.W. and M.F.F.-A, all supervised by J.G. and B.M.-M. C.Y. demonstrated PET-RAFT polymerisation. J.C. performed the optical waveguiding. H.W. and A.M. conducted the P- and SC-XRD analysis. J.-M.H., M.S.K., J.G. and J.K. wrote and edited this manuscript.

Competing interests

The authors declare no competing interests.

Additional information

Supplementary information The online version contains supplementary material available at https://doi.org/10.1038/s41467-025-60316-0.

Correspondence and requests for materials should be addressed to Min Sang Kwon, Johannes Gierschner or Jinsang Kim.

Peer review information *Nature Communications* thanks Dokyoung Kim and the other anonymous reviewer(s) for their contribution to the peer review of this work. A peer review file is available.